Investigating the temperature dependence of the specific shear viscosity of QCD with dilepton radiation

Gojko Vujanovic,[1] Gabriel S. Denicol,[2] Matthew Luzum,[3] Sangyong Jeon,[4] and Charles Gale[4]

[1]*Department of Physics, The Ohio State University, 191 West Woodruff Avenue, Columbus, Ohio 43210, USA*
[2]*Instituto de Física, Universidade Federal Fluminense, UFF, Niterói, 24210-346, RJ, Brazil*
[3]*Instituto de Física - Universidade de São Paulo, Rua do Matão Travessa R, no. 187, 05508-090, Cidade Universitária, São Paulo, Brasil*
[4]*Department of Physics, McGill University, 3600 University Street, Montréal, QC, H3A 2T8, Canada*

This work reports on investigations of the effects on the evolution of viscous hydrodynamics and on the flow coefficients of thermal dileptons, originating from a temperature-dependent specific shear viscosity $\eta/s(T)$ in the quark-gluon plasma (QGP) formed at the Relativistic Heavy-Ion Collider (RHIC). We show that the elliptic flow of thermal dileptons can resolve the magnitude of η/s at the high temperatures probed by the QGP, whereas discriminating between different specific functional forms will likely not be possible at RHIC using this observable.

PACS numbers: 12.38.Mh, 47.75.+f, 47.10.ad

arXiv:1702.02941v1 [nucl-th] 9 Feb 2017

I. INTRODUCTION

Recently, two laboratories – the Relativistic Heavy Ion Collider (RHIC) at the Brookhaven National Laboratory and the Large Hadron Collider at CERN – have created an exotic state of matter: the quark-gluon plasma (QGP). Since this discovery, the characterization of the properties of the QGP has been a mainstream goal of high-energy nuclear physics. One of the striking discoveries of RHIC, also confirmed at the LHC, has been the fluid-dynamical behaviour of the QGP [1, 2]. The progress in hydrodynamic modeling of relativistic heavy-ion collisions has been so rapid over the last decade or so, that there now exists genuine hope to soon be able to precisely quantify the degree of departure for equilibrium of the QGP, by assessing its transport coefficients. Much of the theoretical activity has up to now concentrated on the determination of the shear viscosity to entropy density ratio, as revealed by measurements of the hadronic collectivity [3, 4]. In addition, it is now clear that these same flow data also demand a non-zero value of the specific bulk viscosity, ζ/s [5].

A promising class of probes with which to investigate the QGP directly are electromagnetic (EM) signals, *i.e.* photons and dileptons, as they do not participate in strong interactions can thus escape with negligible final state interactions [6]. Furthermore, these probes are being emitted throughout the entire evolution of the medium, thereby giving local information about the state of the medium, from the initial nucleon-nucleon collisions to kinetic freeze-out. The penetrating nature of EM observables makes them a particularly useful tool to study the temperature-dependence of the transport coefficients of the QCD media. A key coefficient present in all recent hydrodynamical calculations is the shear viscosity η whose temperature-dependence is often assumed to be identical with that of the entropy density s of strongly interacting media, such that η/s is left as a constant to be determined by experimental data. However, it is clear that this is an approximation [7] and in fact, calculations based on perturbative QCD [8], on hadronic degrees of freedom in the confined sector [9–13], and on functional renormalization group techniques [14] show that η/s changes with temperature. Calculations from first principles that address the temperature dependence of η/s are still challenging and it is therefore imperative to investigate whether this information can be extracted from empirical data.

After much work on the extraction of an effective value of η/s in relativistic heavy-ion collisions [2], the temperature-dependence of the η/s ratio has seen increased interest recently, using hadronic observables [15–17] to quantify its behavior. A recent study [18] has shown that the elliptic flow of charged hadrons as a function of transverse momentum at mid-rapidity is sensitive to a temperature-dependent η/s in the hadronic phase both at the top RHIC energy and the LHC, while only LHC data are sensitive to the value of $\eta/s(T)$ in the QGP phase. This investigation continues in the same spirit, but using a complementary EM probe, and focusing on the η/s ratio in the QGP phase. More specifically, the goal of this paper is to explore the sensitivity of thermal dileptons to a temperature-dependent η/s in the QGP phase at top RHIC energy, in order to determine whether thermal dileptons break the degeneracy in $v_2^{ch}(p_T)$ shown in Ref. [18], and further be used to extract the value of the specific shear viscosity, and even possibly of its low order derivatives as a function of T.

This paper is organized as follows: the next section gives the details of the relativistic fluid-dynamical modeling of the strongly-interacting medium. Section III contains a discussion of the lepton pair emission rates in both the QGP and non-perturbative hadronic medium sectors, together with their respective viscous corrections. Results are shown

and discussed in section IV, and are followed by a conclusion.

II. MODELING THE EVOLUTION OF THE MEDIUM CREATED AT RHIC

A. Viscous Hydrodynamics

In this work, we assume that the medium created in relativistic heavy-ion collisions very quickly reaches a state close to thermal equilibrium, such that relativistic dissipative fluid dynamics is a valid description of its space-time behaviour. This assumption is supported by the good agreement between the measured flow coefficients of charged hadrons and the ones calculated through fluid-dynamical simulations (see e.g. [2] for a recent review). In fluid dynamics, the energy-momentum tensor $T^{\mu\nu}$, satisfies the continuity equation,

$$\partial_\mu T^{\mu\nu} = 0, \tag{1}$$

where $T^{\mu\nu} = T_0^{\mu\nu} + \delta T^{\mu\nu}$. Inviscid (ideal) hydrodynamics is contained within $T_0^{\mu\nu}$, which is expressed as $T_0^{\mu\nu} = \varepsilon u^\mu u^\nu - \Delta^{\mu\nu} P$, where ε is the energy density, P the thermodynamic pressure, and $\Delta^{\mu\nu} = g^{\mu\nu} - u^\mu u^\nu$ is the projection operator orthogonal to the 4-velocity u^μ, and $g^{\mu\nu} = \mathrm{diag}\{1, -1, -1, -1\}$. Throughout this study, deviations from ideal hydrodynamics appear exclusively via the shear viscous pressure tensor, i.e. $\delta T^{\mu\nu} = \pi^{\mu\nu}$, with all other dissipative effects being neglected. Furthermore, we set the net baryon 4-current to vanish for all space-time points. The equation of state, which dictates how the thermodynamic pressure changes as a function of energy density, is taken from Ref. [19] and corresponds to a parametrization of a lattice QCD calculation, at high temperatures, smoothly connected to a parametrization of a hadron resonance gas at lower temperatures, which below $T_{\rm ch} = 0.16$ GeV follows a partial chemical equilibrium (PCE) prescription [20, 21].

The dynamics of the shear-stress tensor is given by Israel-Stewart theory [22–24],

$$\tau_\pi \left[\Delta^{\mu\nu}_{\alpha\beta} u^\lambda \partial_\lambda \pi^{\alpha\beta} + \frac{4}{3} \pi^{\mu\nu} \partial_\lambda u^\lambda \right] = 2\eta\sigma^{\mu\nu} - \pi^{\mu\nu}, \tag{2}$$

where $\sigma^{\mu\nu} = \Delta^{\mu\nu}_{\alpha\beta} \partial^\alpha u^\beta$ is the shear tensor and $\Delta^{\mu\nu}_{\alpha\beta} = \frac{1}{2}\left(\Delta^\mu_\alpha \Delta^\nu_\beta + \Delta^\mu_\beta \Delta^\nu_\alpha\right) - \frac{1}{3}\Delta_{\alpha\beta}\Delta^{\mu\nu}$ is the double, symmetric, traceless projection operator. Israel-Stewart theory introduces two transport coefficients, the shear viscosity coefficient (η), which is already present in Navier-Stokes fluid dynamics, and the shear relaxation time, τ_π, germane to Israel-Stewart hydrodynamics. In this study, the relaxation time is fixed at $\tau_\pi = 5\frac{\eta}{\varepsilon + P}$ [25, 26]. In principle, additional nonlinear terms exist in second order dissipative fluid dynamics [25, 26], however we will not be studying their effects here.

Presently, non-perturbative estimates of the aforementioned temperature-dependent transport coefficients in the strongly coupled regime are still a rare commodity [14, 27–29]. Consequently, the growth of the shear viscosity as a function of temperature is modeled by choosing two linear and two quadratic functions of the temperature:

$$\begin{aligned} \frac{\eta}{s}(T) &= m\left(\frac{T}{T_{tr}} - 1\right) + \frac{1}{4\pi}, \\ \frac{\eta}{s}(T) &= a\left(\frac{T}{T_{tr}} - 1\right)^2 + \frac{1}{4\pi} \end{aligned} \tag{3}$$

where $T_{tr} = 0.18$ GeV, while $m = 0.5516, 0.2427$ and $a = 0.4513, 0.1986$ are selected such that $\eta/s = 0.755$ at $T = 0.4$ GeV, and half that value, respectively. Fig. 1 shows all the various forms of temperature dependence used in this calculation. The goal of introducing different temperature-dependent η/s is to investigate the sensitivity of thermal dileptons to this transport coefficient. The fluid-dynamical equations are solved numerically using the MUSIC, which has recently been shown to be in very good agreement with semi-analytic solutions of Israel-Stewart theory [30]. A simulation using $\Delta\tau = 0.03$ fm/c, a grid spacing of $\Delta x = \Delta y = 1/6$ fm, and $\Delta\eta = 1/5$ was precise enough to capture all the relevant physics present in the continuum limit.

B. Initial Conditions and hadronic particle production

As the initial conditions are not currently known in detail, especially those of the shear viscous pressure tensor, we assume that $\pi^{\mu\nu}(\tau_0) \equiv 0$ at $\tau_0 = 0.4$ fm/c when the hydrodynamical evolution begins. Given that the incoming nuclei

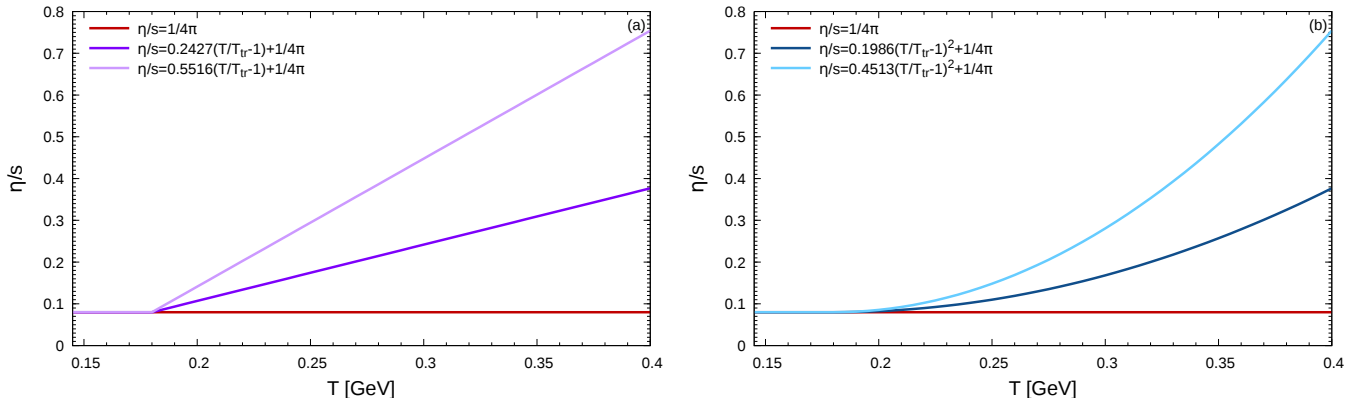

FIG. 1: (Color online) Linear (a) and quadratic (b) temperature dependence of η/s.

have a large longitudinal velocity, while their transverse velocity is assumed to be negligible, we initialize the local fluid velocity u^μ distribution to the Bjorken solution [31]. Thus, we have factorized the initial energy density profile containing a longitudinal part along the space-time rapidity (η_s) direction[1], and transverse part [21] in the transverse (x–y) plane:

$$\varepsilon\left(\tau_0, x, y, \eta_s\right) = \left\{\exp\left[-\frac{\left(|\eta_s| - \eta_{\rm flat}/2\right)^2}{2\eta_\sigma^2}\theta\left(|\eta_s| - \eta_{\rm flat}/2\right)\right]\right\}\left\{W\left[\alpha n_{\rm WN}\left(x,y\right) + \left(1-\alpha\right)n_{\rm BC}\left(x,y\right)\right]\right\}.$$

where the transverse piece being modeled according to the Monte Carlo (MC) Glauber prescription, while $n_{\rm WN}$ is the density of wounded nucleons, $n_{\rm BC}$ is the density of binary collision, W is an overall normalization factor, and α is the proportion in which wounded nucleons and binary collisions contribute to the energy density profile in the transverse plane. The density of wounded nucleons and binary collisions is expressed as

$$n_{\rm BC/WN}\left(x,y\right) = \frac{1}{2\pi\sigma^2}\sum_{i=1}^{N_{\rm bin/part}}\exp\left[-\frac{\left(x-x_i\right)^2+\left(y-y_i\right)^2}{2\sigma^2}\right],$$

where $N_{\rm part}$ and $N_{\rm bin}$ are the number of participants and binary collision of a given event, while (x_i,y_i) are the coordinates of the corresponding participant or binary collision on the transverse plane. In order to determine the number and coordinates of participants and binary collisions, the nucleon-nucleon inelastic cross section, $\sigma_{NN} = 42.1$ mb at $\sqrt{s_{NN}} = 200$ GeV, is used. Table I summarizes the parameters used by the MC Glauber model to describe the charged pion yield and charged hadron elliptic flow at RHIC in the 20–40% centrality class (see also Ref. [32]). Two

TABLE I: Initial state parameters.

Parameter	Value
$\eta_{\rm flat}$	5.9
η_σ	0.4
W	6.16 GeV/fm
α	0.25
σ	0.4 fm

hundred MC Glauber events were generated in this study for each of the four $\eta/s(T)$ functions, along with another two hundred events where $\eta/s = 1/(4\pi)$.

Hadron production proceeds through the Cooper-Frye prescription [33], where the dissipative degrees of freedom are converted to particles through the 14-moments Israel-Stewart (I-S) approximation [34]. The freeze-out temperature

[1] $\eta_s = \frac{1}{2}\ln\left[\frac{t+z}{t-z}\right]$

hypersurface was chosen to be $T_{FO} = 145$ MeV [32] and all 2– and 3–particle decays of hadronic resonances up to 1.3 GeV are computed according to Ref. [35] .

III. THERMAL DILEPTON RATES

Modern equations of state used to describe the medium in relativistic heavy ion collisions, such as the one used in this study, employ a continuous crossover phase transition between the partonic and the hadronic degrees of freedom. In the high temperature regime, perturbative partonic reactions are used to characterize the dilepton production rates, whereas in the low temperature sector, various hadronic interactions are responsible for dilepton radiation. The current calculation follows this prescription and describes the crossover region via a linear interpolation between the high and the low temperature regions, occurring between $0.184 < T < 0.22$ GeV [32].

A. Isotropic (inviscid) dilepton production rates

The general expression for the rates takes an elegant form:

$$\frac{d^4R^{\ell^+\ell^-}}{d^4q} = -\frac{L(M)}{M^2}\frac{\alpha_{EM}^2}{\pi^3}\frac{\mathrm{Im}\Pi_{EM}^R(M,|\mathbf{q}|;T,\mu_B)}{e^{q^0/T}-1} \tag{4}$$

where $\mu_B = 0$ in our hydrodynamical simulation, $M = q_\mu q^\mu$, $q^0 = \sqrt{M^2+\mathbf{q}^2}$, $\alpha_{EM} = \frac{e^2}{4\pi} \approx \frac{1}{137}$, $L(M) = \left(1+\frac{2m_\ell^2}{M^2}\right)\sqrt{1-\frac{4m_\ell^2}{M^2}}$, m_ℓ is the lepton mass, T is the temperature, and $\mathrm{Im}\Pi_{EM}^R$ is the imaginary part of the trace of the retarded (virtual) photon self-energy.

Recently, the perturbative thermal dilepton rates in the QGP have been computed at next-to-leading (NLO) [36–38] within a phenomenologically-interesting kinematic region. In a strongly-coupled setting, the AdS/CFT correspondence has been used to compute emission rates of EM probes from non-Abelian plasmas exhibiting features similar to QCD plasmas [39], while lattice calculations thermal EM production [40, 41] are also available. However, all those rates are currently not amenable to a dissipative description of the medium, hence this study will focus on dilepton rate within the Born approximation.

1. *Dilepton radiation from the QGP*

The Born dilepton rate can be written as:

$$\begin{aligned}\frac{d^4R_0}{d^4q} &= \int \frac{d^3k_1 d^3k_2}{(2\pi)^6 k_1^0 k_2^0} f_{\mathbf{k_1}} f_{\mathbf{k_2}} \frac{q^2}{2}\sigma\delta^4(q-k_1-k_2) \\ \sigma &= \frac{16\pi\alpha_{\rm EM}^2\left(\sum_{f'} e_{f'}^2\right)N_c}{3q^2}\end{aligned} \tag{5}$$

where $f_{\mathbf{k}}$ is the quark/anti-quark distribution functions, σ is the leading-order quark-antiquark annihilation (into a lepton pair) cross section, N_c is the number of colors, the number of flavors is labeled by f' — where only the low-mass ones are considered, i.e. $f' = u, d, s$. Extending the isotropic dilepton rate in Eq. (5) to include shear-viscous effects, amounts to modifying the for quark/anti-quark Fermi-Dirac distribution functions ($f_{\mathbf{k}}$) to include anisotropic deformations. As shear viscosity increases in the QGP sector throughout $\eta/s(T)$, the dilepton rates become more sensitive to the form of the anisotropic correction to the dilepton rate (δR), and a systematic expansion of the anisotropic (or viscous) correction to the Born rates is presented in Section III B.

2. *Dilepton Rates from the anisotropic Hadronic Medium*

In the hadronic sector, we use the Vector meson Dominance Model (VDM), first proposed by Sakurai [42], to relate the virtual photon self-energy $\mathrm{Im}\Pi_{EM}^R$ to the imaginary part of the retarded vector meson propagator $\mathrm{Im}D_V^R$, or,

equivalently, the spectral function:

$$\mathrm{Im}\Pi^R_{EM} = \sum_{V=\rho,\omega,\phi} \left(\frac{m_V^2}{g_V}\right)^2 \mathrm{Im}D^R_V. \tag{6}$$

In the above equation, vector mesons are denoted by $V = \rho, \omega, \phi$, with mass m_V, while their coupling to the photon is g_V. Since the Schwinger-Dyson equation relates the vector meson self-energy to the vector meson spectral function [43], it is sufficient to compute the vector meson self-energy to fully describe medium-induced modifications to vector meson spectral function. Our approach to calculating the vector meson self-energy follows that of by Eletsky *et al.* [44]. The vacuum piece of the self-energy is computed through chiral effective Lagrangians. On the other hand, the finite temperature contribution has been computed through the forward scattering amplitude approach, which includes experimentally observed resonances and Regge physics to account for scattering not going through resonances.

B. A systematic expansion of the anisotropic (viscous) correction to dilepton production rates

Dilepton emission rates were recently extended to take into account deviations from local thermodynamic equilibrium in both the hadronic [45] and QGP sector, the latter being done in the Born limit [46]. Such extensions are essential for a consistent calculation of dilepton production when a viscous fluid describes the evolution of the medium. In those calculations, the authors have generalized the single-quark distribution functions to include anisotropic (viscous) correction using the 14-moment Israel-Stewart (I-S) approximation. In the current calculation, we systematically expand the single-quark momentum distribution function to go beyond the I-S approximation used in [45, 46]. The generalized version of the quark distribution function $f_{\mathbf{k}}$, present in the dilepton rates, takes the form:

$$f_{\mathbf{k}} = \left[\exp\left(y_{\mathbf{k}}\right) + 1\right]^{-1} \tag{7}$$

where $y_{\mathbf{k}} = y(k^\nu, u^\nu; T, \mu)$. Assuming $y_{\mathbf{k}} = y_{0,\mathbf{k}} + \delta y_{\mathbf{k}}$, where $y_{0,\mathbf{k}} = (u^\nu k_\nu - \mu)/T$ and $\delta y_{\mathbf{k}} \ll y_{0,\mathbf{k}}$, we expand Eq. (7) to linear order in $\delta y_{\mathbf{k}}$ obtaining

$$\begin{aligned} f_{\mathbf{k}} &= f_{0,\mathbf{k}} + \delta f_{\mathbf{k}} \\ \delta f_{\mathbf{k}} &= f_{0,\mathbf{k}}\left[1 + a f_{0,\mathbf{k}}\right]\delta y_{\mathbf{k}} \end{aligned} \tag{8}$$

where $f_{0,\mathbf{k}} = \left[\exp\left(y_{0,\mathbf{k}}\right) + 1\right]^{-1}$. $\delta y_{\mathbf{k}}$ can be further expanded as

$$\delta y_{\mathbf{k}} = \mathcal{G}_{\mathbf{k}} \frac{\pi^{\mu\nu} k_\mu k_\nu}{[2T^2(\varepsilon + P)]}, \tag{9}$$

where

$$\mathcal{G}_{\mathbf{k}} = \left[\frac{1 - \tanh(2x - 2x_0)}{2}\right]\mathcal{G}^{\mathrm{low}}_{\mathbf{k}} + \left[\frac{1 + \tanh(2x - 2x_0)}{2}\right]\mathcal{G}^{\mathrm{high}}_{\mathbf{k}}, \tag{10}$$

while $x = \frac{k\cdot u}{T}$ and $x_0 = 11.2$. The formal details of the calculation giving $\mathcal{G}^{\mathrm{low/high}}_{\mathbf{k}}$ are presented in Appendix A; we simply quote the final result:

$$\mathcal{G}^{\mathrm{low/high}}_{\mathbf{k}} = \begin{cases} \frac{5.12}{0.1+x}\left[0.40460300 + 0.15593117x - 0.00740483x^2 + 0.0001693308x^3\right] & \forall x < x_0 \\ \frac{161.8484462}{(0.1+x)^4}\left[-0.25870870 + 0.47053682x - 0.24183275x^2 + 0.065467807x^3\right] & \forall x > x_0 \end{cases}. \tag{11}$$

Given the functional form of $\delta y_{\mathbf{k}}$ is the same as in Ref. [45, 46], the same projection operator can be employed to compute the viscous correction to the dilepton rates. That projection operator is:

$$P_{\alpha\beta} = \frac{1}{2}\frac{g_{\alpha\beta}}{(u\cdot q)^2 - q^2} + \frac{1}{2}\left[\frac{q^2 + 2(u\cdot q)^2}{\left[q^2 - (u\cdot q)^2\right]^2}\right]u_\alpha u_\beta + \frac{3}{2}\frac{q_\alpha q_\beta}{\left[q^2 - (u\cdot q)^2\right]^2} - \frac{3}{2}\left[\frac{u\cdot q}{\left[q^2 - (u\cdot q)^2\right]^2}\right](u_\alpha q_\beta + u_\beta q_\alpha) \tag{12}$$

where q^μ is the four-momentum of the virtual photon. Using $P_{\alpha\beta}$, the viscous correction to the dilepton rate in the local rest frame of the medium is:

$$\begin{aligned} \frac{d^4\delta R}{d^4q} &= \frac{q^\alpha q^\beta \pi_{\alpha\beta}}{2T^2(\epsilon + P)} b_2\left(\frac{q^0}{T}, \frac{|\mathbf{q}|}{T}\right) \\ \frac{d^4\delta R}{d^4q} &= \frac{q^\alpha q^\beta \pi_{\alpha\beta}}{2T^2(\epsilon + P)}\left[C_q \frac{q^2}{2}\frac{\sigma}{(2\pi)^5}\frac{1}{|\mathbf{q}|^5}\int_{E_-}^{E_+} dE_{\mathbf{k}} f_{0,\mathbf{k}}(1 - f_{0,\mathbf{k}}) f_0(q^0 - E_{\mathbf{k}}) D'\right] \end{aligned} \tag{13}$$

where $E_\pm = \frac{q^0 \pm |\mathbf{q}|}{2}$, $f_0(q^0 - E_\mathbf{k}) = \left\{\exp\left[(q^0 - E_\mathbf{k})/T\right] + 1\right\}^{-1}$, $D' = \left[(3q_0^2 - |\mathbf{q}|^2)E_\mathbf{k}^2 - 3q^0 E_\mathbf{k} q^2 + \frac{3}{4}q^4\right]\mathcal{G}_\mathbf{k}$, and $C_q \approx 0.99$. The complete Born rate can therefore be expressed as $\frac{d^4R}{d^4q} = \frac{d^4R_0}{d^4q} + \frac{d^4\delta R}{d^4q}$, where the first and second terms are found in Eq. (5) and Eq. (13), respectively.

To appreciate the improvement the generalized $\delta y_\mathbf{k}$ in Eq. (13) brings relative to the I-S viscous correction, one cannot compare δR to R_0 directly, as the viscous correction depends on the size of $\pi^{\mu\nu}$ at every space-time point. However, one can compare the envelope of the viscous correction b_2 to the ideal rate. So, intuition on the behavior of the viscous correction will instead be acquired through the ratio

$$A\left(\frac{q^0}{T}, \frac{|\mathbf{q}|}{T}\right) = \frac{b_2\left(\frac{q^0}{T}, \frac{|\mathbf{q}|}{T}\right)}{\frac{d^4R_0}{d^4q}} \tag{14}$$

evaluated in the local rest frame. The ratio A has a very weak dependence on $\frac{|\mathbf{q}|}{T}$, hence evaluating it at $\frac{|\mathbf{q}|}{T} = 0$ is sufficient. Fig. 2 clearly shows that A for the I-S viscous correction is bounded between $\frac{1}{3}$ and $\frac{2}{3}$. Since $\frac{q^\alpha q^\beta \pi_{\alpha\beta}}{2T^2(\epsilon+P)}$ is

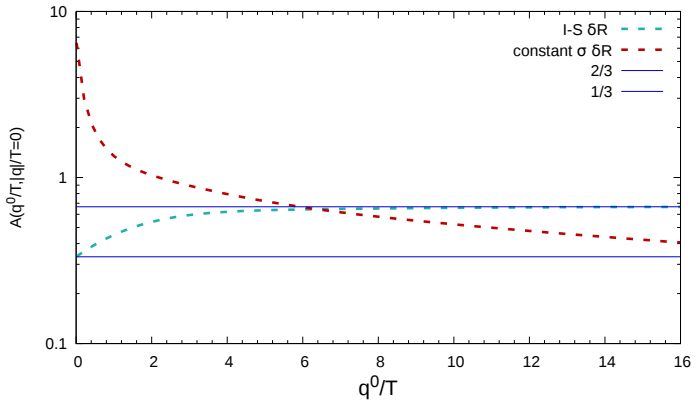

FIG. 2: (Color online) Relative size of the envelope of the viscous correction relative to the (ideal) isotropic rate in the local rest frame.

well behaved in the vanishing q^μ limit, the lower bound on A is not a source of concern. Using only the upper bound, the I-S correction to the QGP dilepton rate becomes ill-behaved when $\frac{q^\alpha q^\beta \pi_{\alpha\beta}}{2T^2(\epsilon+P)} > \frac{3}{2}$. In that respect, the viscous correction that we have computed is better behaved at large $\frac{q^0}{T}$ as $A \sim \left(\frac{q^0}{T}\right)^{-1}$, and is furthermore is finite at $\frac{q^0}{T} = 0$. This suppression at large $\frac{q^0}{T}$ is needed to ensure that δR is well behaved when a large $\pi^{\mu\nu}$ is present, due to a $\eta/s(T)$. The effects of the constant cross section anisotropic δR correction and the I-S δR on the dilepton differential yield will be explored in Appendix B.

In the Hadronic Medium (HM), the viscous correction to the dilepton rates are accounted for through a modification of the vector meson self-energy. The full self-energy Π contains two pieces $\Pi = \Pi_0 + \delta\Pi$. Π_0 is the isotropic contribution that is described in Section III A 2, while $\delta\Pi$ is the anisotropic one that accounts for quadrupole deformations (see Appendix A) induced by the shear-stress tensor $\pi^{\mu\nu}$ (see [45] for details). Since $\delta\Pi$, originating from the I-S viscous correction to the thermal distribution, is a very steeply falling function of (M, $\mathbf{q}$) [45], there is no need to devise a different viscous correction.

IV. RESULTS

Before disclosing the effects of $\eta/s(T)$ on dilepton flow, it is important to specify the manner in which dilepton flow coefficients are computed. We use the scalar product method:

$$v_n^{\gamma^*} = \frac{\left\langle v_n^h v_n^{\gamma^*} \cos\left[n\left(\Psi_n^{\gamma^*} - \Psi_n^h\right)\right]\right\rangle_{\rm ev}}{\sqrt{\langle (v_n^h)^2\rangle_{\rm ev}}} \tag{15}$$

where $\langle \ldots \rangle_{\rm ev}$ is an average over events[2]. In single event, the hadronic v_n^h and Ψ_n^h are given by

$$v_n^h e^{in\Psi_n^h} = \frac{\int dp_T dy d\phi p_T \left[p^0 \frac{d^3N^h}{d^3p}\right] e^{in\phi}}{\int dp_T dy d\phi p_T \left[p^0 \frac{d^3N^h}{d^3p}\right]} \tag{16}$$

where the charged hadron distribution is integrated over $-0.35 < \eta < 0.35$ and $0.035 < p_T < 3$ GeV to simulate acceptance used by the PHENIX experiment at RHIC. The dilepton $v_n^{\gamma^*}$ and $\Psi_n^{\gamma^*}$ are computed using the same approach, with the more general distribution $\frac{d^4N^{\gamma^*}}{d^4p}$.

A. Linear $\eta/s(T)$

The goal of this section is to investigate the sensitivity of thermal dileptons to the size of $\eta/s(T)$'s slope. Since the effects a temperature dependent η/s induces on the evolution of the medium are rather complicated, keeping identical initial/freeze-out conditions, regardless of any entropy production that $\eta/s(T)$ introduces, is important for the purpose of a comparison. Furthermore, since the amount of entropy generation is smaller than the effects $\eta/s(T)$ instigates on the anisotropic evolution of the system, compensating for entropy production by changing in initial/freeze-out conditions is not mandatory.

To quantify the amount of entropy, radial flow generated via a linearly dependent $\eta/s(T)$, as well as the importance of δn effects, the yield of thermal dileptons as a function of M and the yield of pions as a function of p_T is plotted in Fig. 3. The invariant mass thermal dilepton yield is very slightly modified owing to $\eta/s(T)$ as seen in Fig. 3 (a).

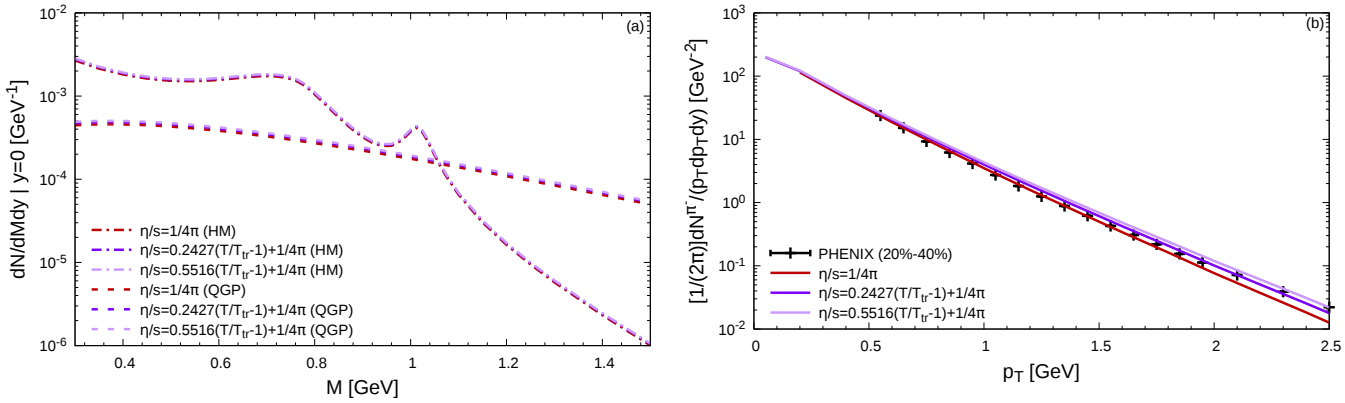

FIG. 3: (Color online) Yield of thermal dileptons (a) and pions (b) for various values of $\eta/s(T)$.

Indeed, the yield is increased by 5% in the HM region while the QGP region receives an increase of 10%. Since M is a Lorentz-invariant quantity, the increase in the invariant mass yield is a measure of the entropy production of a dissipative system. The somewhat larger increase in the pion yield at higher $p_T \gtrsim 1$ GeV [see Fig. 3 (b)] is explained by a combination of a greater radial flow and larger δn effects when $\eta/s(T)$ is present, while at low $p_T \lesssim 1$ GeV greater entropy production and radial flow give the increase in pion yield. However, this larger radial flow is not affecting the elliptic flow of charged hadrons at RHIC energies as can be seen in Fig. 4 (a), and was first noticed in Ref. [18]. On the other hand, a linearly dependent $\eta/s(T)$ changes the flow of thermal dileptons quite substantially [see Fig. 4 (b)], and can potentially be measured in experiment. This behavior of thermal dilepton's $v_2(M)$ can be explained by the difference in the evolution in the HM and QGP sectors. Such a different evolution in the partonic and hadronic sector may appear to be somewhat surprising as the temperature-dependent η/s is present (mostly) in the QGP. However, as we explore the anisotropic flow build-up in the HM and QGP sectors, and the manner in which this affects the overall evolution of the system, it will become clear how the evolution in the QGP influences the later evolution of the HM.

---

[2] Note that according to Eq. (15), the v_2 of charged hadrons corresponds to the root mean square value of the hydrodynamical events sampled.

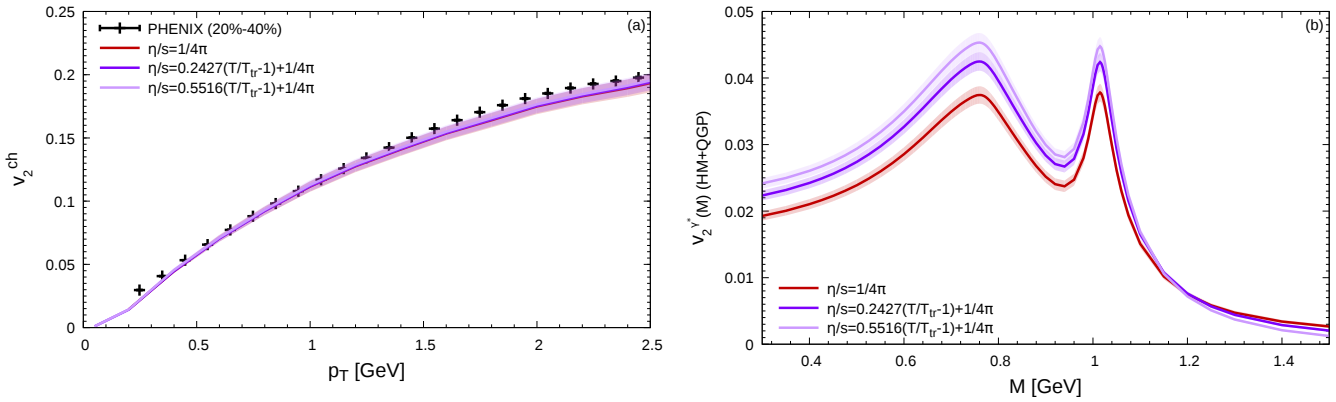

FIG. 4: (Color online) Elliptic flow of charged hadrons (a) and thermal dileptons (b) with different slopes of $\eta/s(T)$. The colored bands represent the statistical error associated with the 200 events used in this study.

As a first step in this direction, the HM and QGP contributions are presented individually in Fig. 5. The elliptic

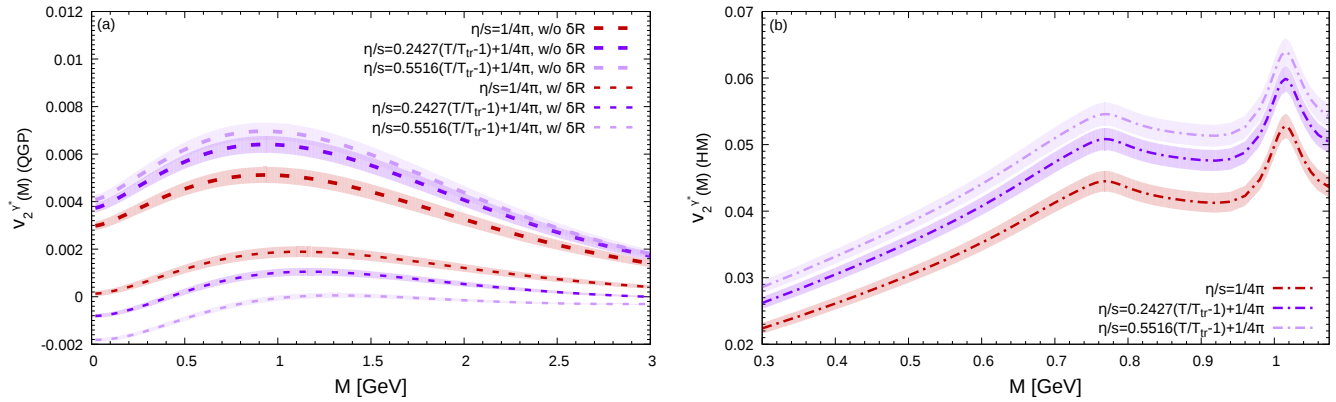

FIG. 5: (Color online) Elliptic flow of QGP (a) and HM (b) dileptons with different slopes of $\eta/s(T)$.

flow of the QGP in Fig. 5 (a) without viscous correction δR, is increased with $\eta/s(T)$, owing to the fact that (i) $\pi^{\mu\nu}$ at early times increases the transverse velocity gradients of the fluid and (ii) R_0 solely couples to fluid velocity u^μ and temperature T and hence is directly sensitive to increase in velocity gradients. On the other hand, δR couples to $\pi^{\mu\nu}$ in addition to u^μ and T, and is responsible for decreasing the elliptic flow as shown in Ref. [45] (and references therein). This is also confirmed in Fig. 6 (a), where ideal $T^{\mu\nu}$ refers to the momentum anisotropy $\langle T^{xx} - T^{yy}\rangle/\langle T^{xx} + T^{yy}\rangle$ computed using only $T_0^{\mu\nu}$ of a viscous evolution, while the full $T^{\mu\nu}$ curves also include $\pi^{\mu\nu}$.

The fact that $v_2(M)$ of QGP dileptons goes negative comes from the fact that the event plane angle for QGP dileptons is misaligned with that of charged hadrons. Indeed, if $\pi/2 < n(\Psi_n^{\gamma^*} - \Psi_n^h) < 3\pi/2$, any flow harmonic will automatically become negative. This misalignment between the angles $\Psi_n^{\gamma^*}$ and Ψ_n^h is evident in Fig. 6 [see curves labeled full $T^{\mu\nu}$ in (a) and (b)] and is responsible for the driving the $v_2(M)$ of QGP dileptons to negative values.[3] Indeed, Fig. 6 (a) shows that the development of flow anisotropy in the QGP sector is reduced in the cases where η/s is temperature-dependent (see curves labeled Full $T^{\mu\nu}$), while Fig. 6 (b) shows that in the hadronic sector $\eta/s(T)$ causes an increase in the anisotropic flow development, and this anticorrelation is causing large differences between $\Psi_n^{\gamma^*}$ and Ψ_n^h, which is driving v_2 of QGP dileptons to negative values. Physically, a medium with a large viscosity at large temperatures is postponing the conversion of the original geometrical anisotropy of the QGP region into a momentum anisotropy. So for the first 1.5 fm/c of evolution the QGP with a temperature dependent η/s develops

[3] Note that the misalignment is captured by δR.

anisotropic flow slower than the QGP with a constant η/s, as seen in Fig. 6 (a) using the full $T^{\mu\nu}$. Furthermore, the medium with $\eta/s(T)$ has more entropy production at early times that the one with $\eta/s = 1/(4\pi)$. These two effects are consistent with the observation that a medium with $\eta/s(T)$ in the QGP will cool slower at early times than the one with $\eta/s = 1/(4\pi)$, as seen in Fig. 7 (a).

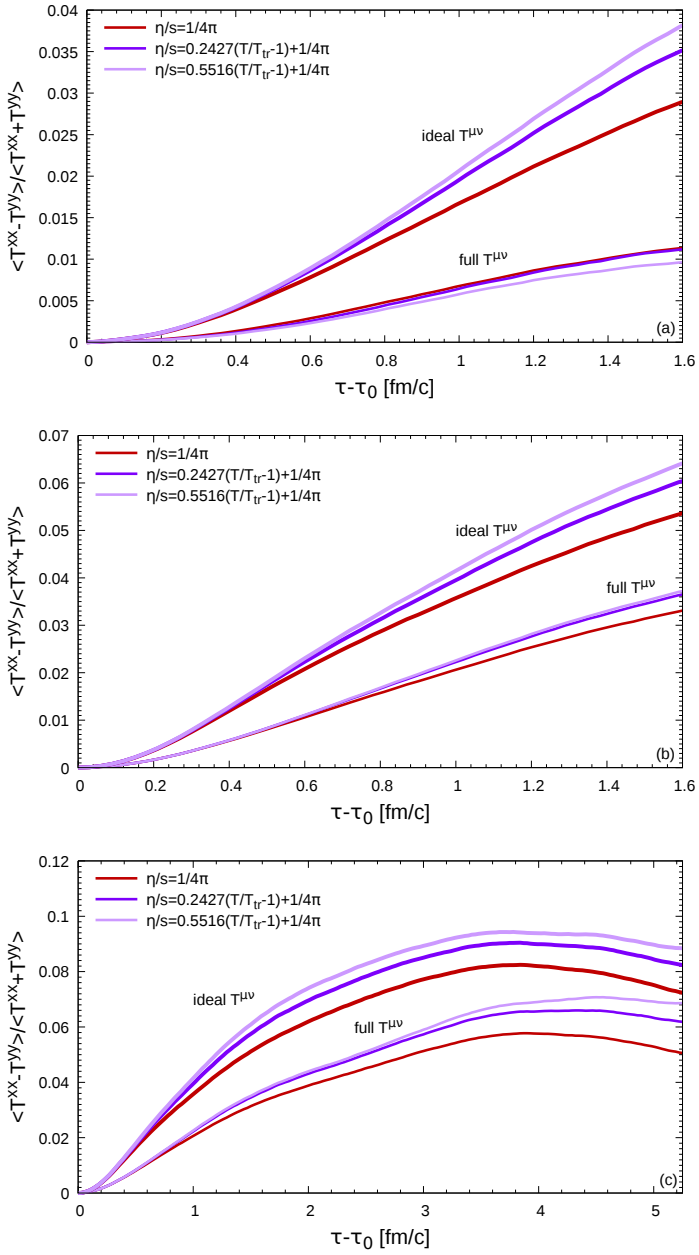

FIG. 6: (Color online) Momentum anisotropy of the fluid. The QGP is in (a), the HM sector at early times is in (b), while (c) shows the HM anisotropy evolution for a larger time span. The meaning of ideal/full $T^{\mu\nu}$ is explained in the text. The momentum anisotropy of the QGP/HM was obtained after integrating over *all* fluid cells in the QGP/HM sectors and averaging over 200 hydro events.

However, such a situation cannot be maintained indefinitely, since the hotter media (with $\eta/s(T)$) will exert more pressure than the one with $\eta/s = 1/(4\pi)$. So, as soon as the viscosity is low enough for the anisotropic pressure gradients to start developing anisotropic flow, which happens between 1.5 – 2.5 fm/c in our calculation [see Fig. 7 (b)], the fluids with $\eta/s(T)$ will start cooling faster than the one with $\eta/s = 1/(4\pi)$, and ultimately will freeze-out sooner [see Fig. 7 (c)]. This late anisotropic push of the $\eta/s(T)$ medium results in a higher $v_2(M)$ of HM dileptons

as can be seen in Fig. 5 (b). Note that the flow harmonics of HM dileptons are little affected by a viscous correction δR [45] and Fig. 5 (b) is showing a calculation with δR. Hence, HM dileptons are tracking more closely the build-up of the momentum anisotropy originating from the ideal part of $T^{\mu\nu}$, while QGP dileptons track the full momentum anisotropy in Fig. 6.

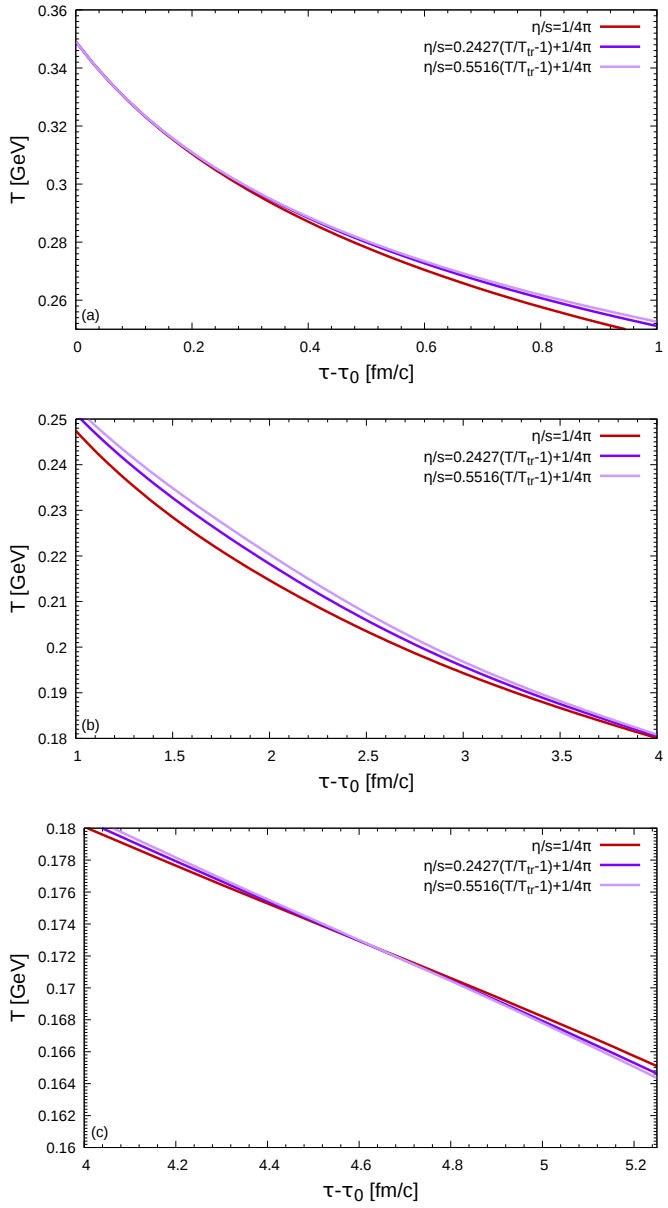

FIG. 7: (Color online) Event-averaged temperature for the cell (x,y,z)=(0,0,0) during the first fm/c of evolution (a) and at later stages (b–c).

As confirmation that HM dileptons are experiencing a greater push at late stages of the evolution, we plot in Fig. 8 the temperature profile in the transverse plane at late time. The medium with a $\eta/s(T)$ produces a more elongated shape than $\eta/s = 1/(4\pi)$, see Fig. 8 (a) and (b), respectively. Of course, in both cases, the initial condition explained in Section II B was used.

For the charged hadron v_2 to be consistent with this picture, the shape of the freeze-out hypersurface should not vary significantly between $\eta/s(T)$ and $\eta/s = 1/(4\pi)$, as can be seen in Fig. 9. Hence, given that the freeze-out temperature is fixed to $T_{FO} = 145$ MeV, the larger anisotropic push generated by a temperature-dependent η/s, didn't have enough time to significantly affect the flow anisotropy on the freeze-out hypersurface before freeze-out

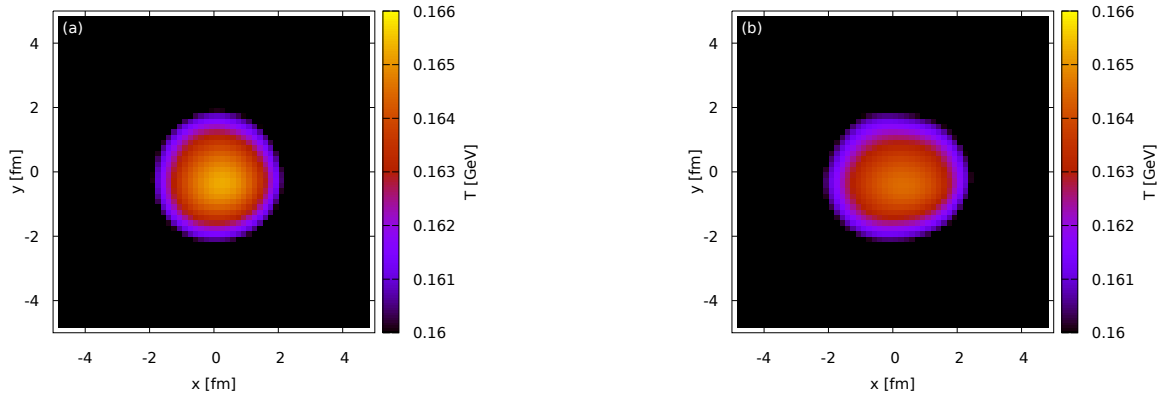

FIG. 8: (Color online) Event-averaged temperature in the transverse plane at $z = 0$ at $(\tau - \tau_0) = 5.25$ fm/c for $\frac{\eta}{s} = \frac{1}{4\pi}$ (a) and $\frac{\eta}{s} = 0.4513\left(\frac{T}{T_{tr}} - 1\right) + \frac{1}{4\pi}$ (b).

occurs.

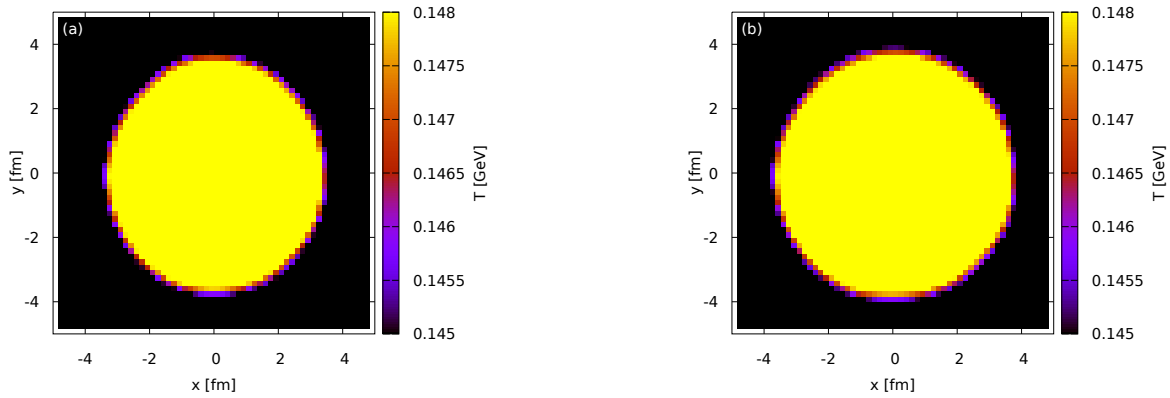

FIG. 9: (Color online) Event-averaged temperature in the transverse plane at $z = 0$ at $(\tau - \tau_0) = 5.25$ fm/c for $\frac{\eta}{s} = \frac{1}{4\pi}$ (a) and $\frac{\eta}{s} = 0.4513\left(\frac{T}{T_{tr}} - 1\right) + \frac{1}{4\pi}$ (b) near the freeze-out surface boundary.

Given the sizable elliptic and triangular flow of thermal dileptons as a function of p_T (see Fig. 10), the p_T-differential flow harmonics also bear promise to potentially constrain, in experimental data, the slope of $\eta/s(T)$. Indeed to maximize this opportunity, the invariant mass M was chosen in a region where the thermal radiation dominates over all other sources [45]. In particular, notice the difference in the p_T-dependence of flow harmonics — especially $v_2(p_T \gtrsim 2$ GeV) and $v_3(p_T \gtrsim 3$ GeV) – when a temperature-dependent η/s is being used. Such a prominent variation is ideal if slope of $\eta/s(T)$ is to be experimentally constrained.

B. Quadratic $\eta/s(T)$

We now turn our attention towards the second derivative of $\eta/s(T)$. The initial and freeze-out conditions are unchanged. The amount of entropy production for a quadratic $\eta/s(T)$ depicted in Fig. 11 (a) is even smaller than that of a linear $\eta/s(T)$. The dilepton yield is only increased by about 2% in the HM and 6% in the QGP regions, respectively. In addition, the amount of radial flow has been reduced compared to the linear $\eta/s(T)$ [see Fig. 11 (b)]. As before, the charged hadron elliptic flow is not affected by $\eta/s(T)$, while elliptic flow of thermal dileptons is [see Fig. 12].

Since the invariant mass distribution of thermal dilepton $v_2(M)$ for a quadratic $\eta/s(T)$ is similar to a linear $\eta/s(T)$, the transverse momentum distribution of dilepton flow harmonics are a more interesting quantity, as they may have

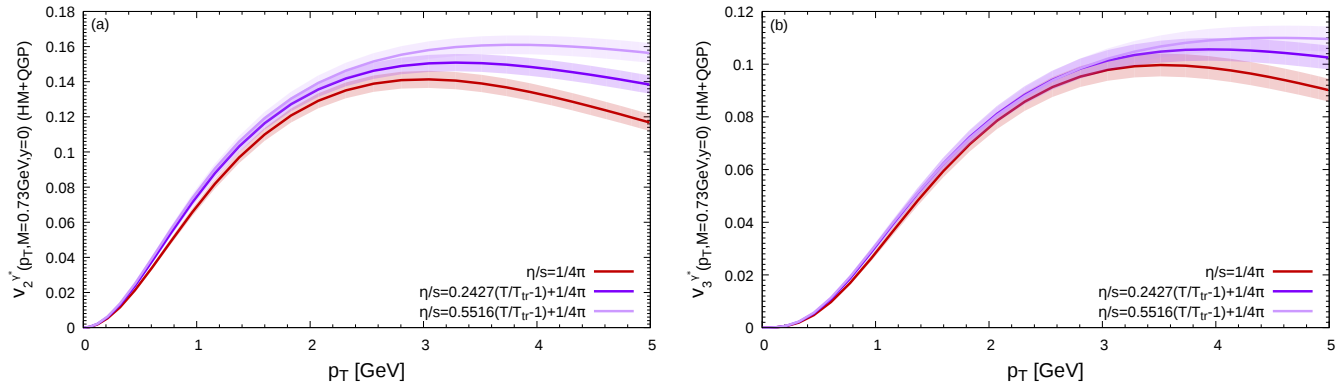

FIG. 10: (Color online) Elliptic (a) and triangular (b) flow of thermal dileptons for a linearly dependent $\eta/s(T)$.

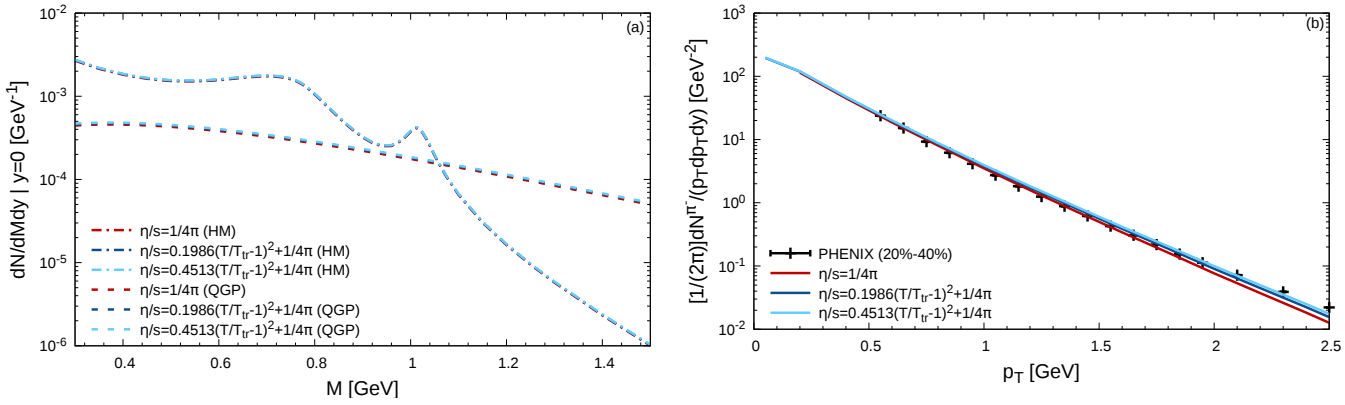

FIG. 11: (Color online) Yield of thermal dileptons (a) and pions (b) for various values of $\eta/s(T)$.

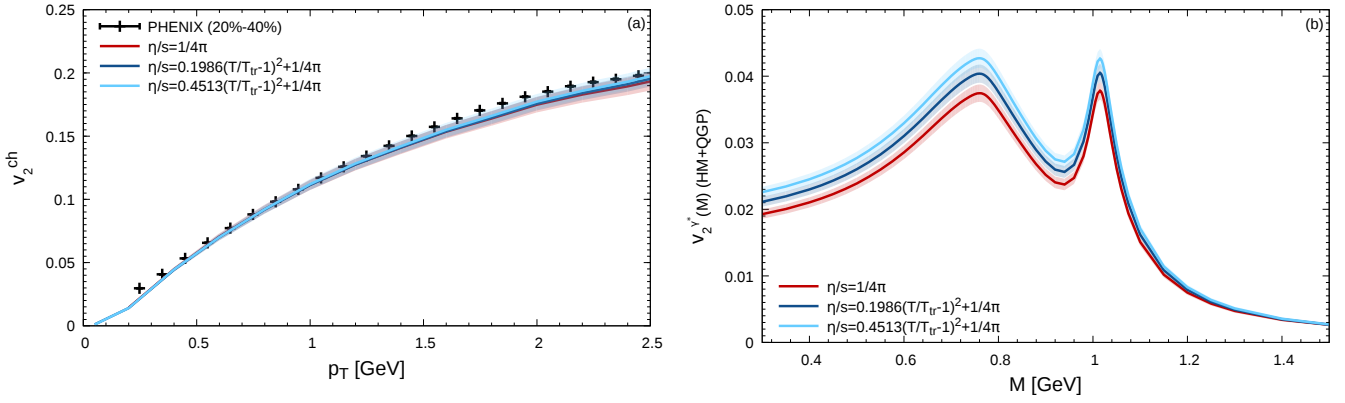

FIG. 12: (Color online) Elliptic flow of charged hadrons (a) and thermal dileptons (b) with different slopes of $\eta/s(T)$.

more discriminating power regarding whether $\eta/s(T)$ is linear or quadratic.

The transverse momentum distribution displays some sensitivity to whether $\eta/s(T)$ is linear or quadratic. Indeed, at intermediate invariant masses, Fig. 13 shows that $v_2(p_T)$ can clearly distinguish between the two functional forms for $\eta/s(T)$. At low invariant masses, higher flow harmonics do show a moderate difference going from linear to quadratic $\eta/s(T)$ at $p_T \gtrsim 3$ GeV [see Fig. 14], which cannot be accounted for through a renormalization of the slope alone. Unfortunately, experimentally distinguishing between the two forms of $\eta/s(T)$ will be challenging at RHIC

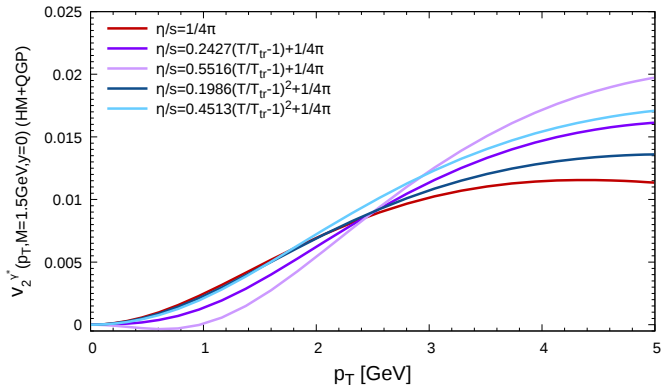

FIG. 13: (Color online) A comparison of v_2 of thermal dileptons using linear and quadratic $\eta/s(T)$ at an intermediate invariant mass. The uncertainties associated with the 200 events generated were removed to improve visual clarity.

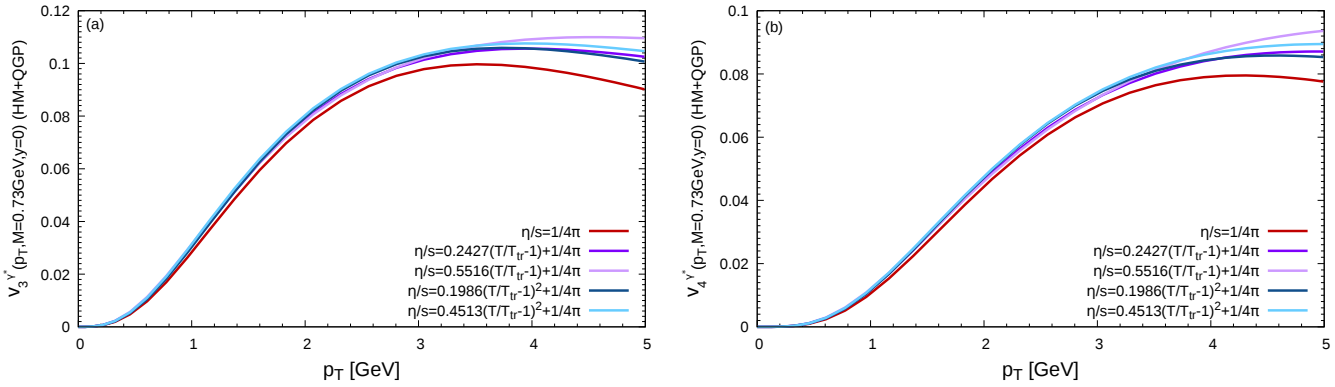

FIG. 14: (Color online) A comparison of v_3 (a) and v_4 (b) of thermal dileptons using linear and quadratic $\eta/s(T)$ at low invariant mass. The uncertainties associated with the 200 events generated were removed to improve visual clarity.

given the sensitivity required, be it in the overall magnitude of the signal or in the relative difference between signals. Thus studying dilepton flow at LHC energies could be more promising and such a study is currently underway.

V. CONCLUSIONS

The goal of the present work is to investigate the sensitivity of thermal dileptons to a temperature-dependent η/s in the QGP, at top RHIC energy. We have studied the sensitivity of dilepton flow to the slope of a linearly dependent $\eta/s(T)$ and the size of its second derivative with respect to temperature. Hadronic observables are found to be poorly sensitive to any temperature dependence, be it linear or quadratic, of η/s in the QGP sector, as was previously found in Ref. [18]. We have shown that dileptons have sensitivity to a temperature-dependent η/s.

The STAR Collaboration at RHIC has recently acquired new dilepton data using its Muon Telescope Detector (MTD) and Heavy Flavor Tracker (HFT) [47]. Having the HFT running at the same time, allows to remove the dilepton radiation coming from open heavy flavor hadrons in the low to intermediate invariant mass (i.e. $M \lesssim 2.5$ GeV), thus allowing to directly measure thermal dilepton radiation for $M \lesssim 2.5$ GeV and compare to to the results presented herein. The analysis of these dilepton data using the MTD and the HFT detectors at STAR is currently ongoing [47], with improved dileptons measurements of v_2 expected soon. As shown here, the ability to measure $v_2(M)$ of thermal dileptons opens the possibility of using thermal dileptons to resolve details in the overall magnitude of $\eta/s(T)$ of the QGP. Thus, extracting the temperature-dependence of η/s via dileptons seems to be a very promising prospect at RHIC. LHC on the other hand, does not currently have the capabilities in place to accurately measure low to intermediate mass dileptons, with such measurements only being possible once the LHC detector upgrades are

in place [48].

Though both the slope or the size of the second derivative did influence the magnitude and shape of the dilepton flow harmonics, with appreciable effects on $v_2(M)$, distinguishing between a linear versus quadratic temperature dependence would be difficult at RHIC for $M \lesssim 2.5$ GeV. Indeed, at fixed low invariant mass, though the shape of $v_3(p_T)$ and $v_4(p_T)$ is different within the a linear and quadratic temperature dependence of η/s, that difference only becomes apparent at high transverse momenta. At intermediate invariant masses, while the shape of $v_2(p_T)$ is more pronounced when going from a linear to a quadratic $\eta/s(T)$, the overall magnitude of the signal is significantly smaller. Given the differential nature of the $v_2(M, p_T)$ measurement, extracting the signal with enough statistics to be able to distinguish between a linear or quadratic $\eta/s(T)$ is experimentally challenging at low and intermediate invariant masses. Thus, the currently most promising dilepton candidate learn about the temperature-dependence of η/s is $v_2(M)$.

Acknowledgments

We are grateful to J.-F. Paquet, C. Shen, and B. Schenke for helpful discussions. This work was supported in part by the Natural Sciences and Engineering Research Council of Canada, in part by the Director, Office of Energy Research, Office of High Energy and Nuclear Physics, Division of Nuclear Physics, of the U.S. Department of Energy under Contracts No. DE-AC02-98CH10886, DE-AC02-05CH11231, and DE-SC0004286, and in part by the National Science Foundation (in the framework of the JETSCAPE Collaboration) through award number 1550233. G. Vujanovic acknowledges support by the Fonds de Recherche du Québec — Nature et Technologies (FRQNT), the Canadian Institute for Nuclear Physics, and by the Seymour Schulich Scholarship, while G.S. Denicol acknowledges support through a Banting Fellowship from the Government of Canada. Computations were performed on the Guillimin supercomputer at McGill University under the auspices of Calcul Québec and Compute Canada. The operation of Guillimin is funded by the Canada Foundation for Innovation (CFI), the Natural Sciences and Engineering Research Council (NSERC) of Canada, NanoQuébec, and the Fonds de Recherche du Québec— Nature et Technologies (FRQNT).

Appendix A: Computing the viscous correction to the QGP rate via the Boltzmann Equation

The discussion presented here follows Ref. [26]. In order to derive the $\delta n_{\mathbf{k}}$ used in Eq. (11), the starting point is

$$\delta y_{\mathbf{k}} = \mathscr{G}_{\mathbf{k}} \phi_{\mathbf{k}} \tag{A1}$$

where $\phi_{\mathbf{k}}$ is be computed after performing an irreducible tensor decomposition and $\mathscr{G}_{\mathbf{k}}$ is an arbitrary function of $k^\mu u_\mu$. Indeed, one can decompose $\phi_{\mathbf{k}}$ as

$$\phi_{\mathbf{k}} = \lambda_{\mathbf{k}}^{(0)} + \sum_{\ell=1}^{\infty} \lambda_{\mathbf{k}}^{\langle \mu_1 \ldots \mu_\ell \rangle} k_{\langle \mu_1} \ldots k_{\mu_\ell \rangle} \tag{A2}$$

where $\lambda_{\mathbf{k}}^{\langle \mu_1 \ldots \mu_\ell \rangle} = \Delta^{\mu_1 \ldots \mu_\ell}_{\nu_1 \ldots \mu_{\ell'}} \lambda_{\mathbf{k}}^{\nu_1 \ldots \nu_{\ell'}}$ with $\Delta^{\mu_1 \ldots \mu_\ell}_{\nu_1 \ldots \mu_{\ell'}}$ being defined in Ref. [26, 49]. For $\ell = 1$ and $\ell = 2$, the irreducible tensor $\Delta^{\mu_1 \ldots \mu_\ell}_{\nu_1 \ldots \mu_{\ell'}}$ simplifies to Δ^{μ}_{ν}, and $\Delta^{\mu\nu}_{\alpha\beta}$, respectively. These two tensors were defined in section II A. The tensors $\lambda_{\mathbf{k}}^{\langle \mu_1 \ldots \mu_\ell \rangle}$, being expanded in terms of the mutually orthogonal irreducible tensors $k_{\langle \mu_1} \ldots k_{\mu_\ell \rangle}$, can be further factorized into a linear combination of an orthonormal set of functions $P^{(\ell)}_{n,\mathbf{k}}$, that explicitly depend on $E_{\mathbf{k}} = u^\nu k_\nu$, and a set of rank-$\ell$ tensor coefficient $c_n^{\langle \mu_1 \ldots \mu_\ell \rangle}$ as

$$\lambda_{\mathbf{k}}^{\langle \mu_1 \ldots \mu_\ell \rangle} = \sum_{n=0}^{N_\ell} c_n^{\langle \mu_1 \ldots \mu_\ell \rangle} P^{(\ell)}_{n,\mathbf{k}}. \tag{A3}$$

So, the expansion basis of the tensorial structure of $\phi_{\mathbf{k}}$ are $k_{\langle \mu_1} \ldots k_{\mu_\ell \rangle}$, which, analogous to spherical harmonics, contain the angular dependence of $\phi_{\mathbf{k}}$. The expansion coefficients are $c_n^{\langle \mu_1 \ldots \mu_\ell \rangle}$. Using the spherical harmonics analogy, $\lambda_{\mathbf{k}}^{(0)}$, $\lambda_{\mathbf{k}}^{\langle \mu_1 \rangle}$, and $\lambda_{\mathbf{k}}^{\langle \mu_1 \mu_2 \rangle}$ can be interpreted as monopole, dipole, and quadrupole contributions to $\phi_{\mathbf{k}}$, respectively, and so on for the higher order tensors. The irreducible tensors $k_{\langle \mu_1} \ldots k_{\mu_\ell \rangle}$ satisfy the orthogonality condition

$$\int dK n_{\mathbf{k}} k_{\langle \mu_1} \ldots k_{\mu_\ell \rangle} k^{\langle \mu_1} \ldots k^{\mu_{\ell'} \rangle} = \frac{\ell!(2\ell+1)\delta_{\ell\ell'}}{(2\ell+1)!!} \int dK (\Delta^{\alpha\beta} k_\alpha k_\beta)^\ell n_{\mathbf{k}} \tag{A4}$$

where

$$\int dK \equiv \int \frac{d^4k}{(2\pi)^4}\delta\left(k^\nu k_\nu - m^2\right)\theta\left(k^0\right). \tag{A5}$$

On the other hand, $\phi_{\mathbf{k}}$'s radial dependence is expanded using the orthonormal basis functions $P^{(\ell)}_{n,\mathbf{k}}$, which can be written as

$$P^{(\ell)}_{n,\mathbf{k}} = \sum_{r=0}^{n} a^{(\ell)}_{n,r} E^r_{\mathbf{k}}. \tag{A6}$$

The orthonormal basis functions $P^{(\ell)}_{n,\mathbf{k}}$ satisfy

$$\int dK P^{(\ell)}_{n,\mathbf{k}} P^{(\ell)}_{m,\mathbf{k}} \omega^{(\ell)} = \delta_{mn} \tag{A7}$$

where

$$\omega^{(\ell)} = \frac{(-1)^\ell}{(2\ell+1)!!} \frac{(\Delta^{\alpha\beta}k_\alpha k_\beta)^\ell (1-n_{0,\mathbf{k}}) n_{0,\mathbf{k}} \mathscr{G}_{\mathbf{k}}}{\int dK (-\Delta^{\alpha\beta}k_\alpha k_\beta)^\ell n_{0,\mathbf{k}}(1-n_{0,\mathbf{k}})\mathscr{G}_{\mathbf{k}}} \tag{A8}$$

and has the property $\int dK \omega^{(\ell)} = 1$. Being interested in computing $\delta y_{\mathbf{k}}$ for shear viscous stresses, the only term needed is $\ell = 2$. Thus $\delta y_{\mathbf{k}}$ can be expressed as

$$\delta y_{\mathbf{k}} = \mathscr{G}_{\mathbf{k}} \sum_{n=0}^{N_2} P^{(2)}_{n,\mathbf{k}} c^{\langle\mu\nu\rangle}_n k_{\langle\mu} k_{\nu\rangle}. \tag{A9}$$

where, using the orthogonality condition of the irreducible tensors,

$$c^{\langle\mu\nu\rangle}_n = \frac{1}{2!} \frac{\int dK \mathscr{G}_{\mathbf{k}} P^{(2)}_{n,\mathbf{k}} k^{\langle\mu} k^{\nu\rangle} \delta n_{\mathbf{k}}}{\int dK (-\Delta^{\alpha\beta}k_\alpha k_\beta)^2 n_{0,\mathbf{k}}(1-n_{0,\mathbf{k}})\mathscr{G}_{\mathbf{k}}}. \tag{A10}$$

It is convenient to re-express $\delta y_{\mathbf{k}}$ in terms of irreducible moments of $\delta n_{\mathbf{k}}$,

$$\rho^{\mu\nu}_n = \int dK E^n_{\mathbf{k}} k^{\langle\mu} k^{\nu\rangle} \delta n_{\mathbf{k}} \tag{A11}$$

such that

$$\delta n_{\mathbf{k}} = n_{0,\mathbf{k}}(1-n_{0,\mathbf{k}})\mathscr{G}_{\mathbf{k}} \sum_{n=0}^{N_2} \mathcal{H}^{(2)}_{n,\mathbf{k}} \rho^{\mu\nu}_n k_{\langle\mu} k_{\nu\rangle} \tag{A12}$$

where

$$\mathcal{H}^{(2)}_{n,\mathbf{k}} = \frac{1}{2!} \frac{\sum_{m=n}^{N_2} a^{(2)}_{mn} P^{(2)}_{m,\mathbf{k}} \mathscr{G}_{\mathbf{k}}}{\int dK (-\Delta^{\alpha\beta}k_\alpha k_\beta)^2 n_{0,\mathbf{k}}(1-n_{0,\mathbf{k}})\mathscr{G}_{\mathbf{k}}} \tag{A13}$$

At this point, we have expressed $\delta n_{\mathbf{k}}$ in terms of its moments $\rho^{\mu\nu}_n$. However, only the lowest of these moments, $\rho^{\mu\nu}_0 = \pi^{\mu\nu}$, are described within hydrodynamics. In order to apply this formula to describe the momentum distribution of particles within a fluid, it is still necessary to approximate the remaining moments in terms of the fluid dynamical degrees of freedom. In the hydrodynamical limit, one can assume that all moments $\rho^{\mu\nu}_n$ have sufficiently approached their asymptotic values and have relaxed to their Navier-Stokes limit. That is,

$$\rho^{\mu\nu}_n \;\approx\; 2\eta_n \sigma^{\mu\nu}. \tag{A14}$$

With this approximation it becomes possible to express all moments $\rho^{\mu\nu}_n$ in terms of $\pi^{\mu\nu}$, in the following way:

$$\rho^{\mu\nu}_n \approx \frac{\eta_n}{\eta}\pi^{\mu\nu}, \tag{A15}$$

where we have used the Navier-Stokes limit for $\pi^{\mu\nu}$, namely $\pi^{\mu\nu} = 2\eta\sigma^{\mu\nu}$. Here, η_n is a set of transport coefficients which contain the microscopic information of the system. In fact, η_0 is nothing but the usual shear viscosity coefficient η already discussed. The remaining transport coefficients are less known, but can be calculated within the framework of the Boltzmann equation (or Kinetic Theory). An estimate of these transport coefficients was derived in Ref. [25] within the Boltzmann equation, assuming the colliding quarks are massless and that their $2 \to 2$ scattering cross section is constant.[4] The final expression for $\delta n_{\mathbf{k}}$ then becomes:

$$\delta n_{\mathbf{k}} = n_{0,\mathbf{k}}(1 - n_{0,\mathbf{k}})\mathscr{G}_{\mathbf{k}} \left[\sum_{n=0}^{N_2} H^{(2)}_{n,\mathbf{k}} \frac{\eta_n}{\eta}\right] \frac{\pi^{\mu\nu}}{2(\varepsilon + P)} \frac{k_\mu}{T} \frac{k_\nu}{T}, \tag{A16}$$

where $\mathcal{G}_{\mathbf{k}} = \mathscr{G}_{\mathbf{k}} \left[\sum_{n=0}^{N_2} H^{(2)}_{n,\mathbf{k}} \frac{\eta_n}{\eta}\right]$, and the temperature dependence was introduced by replacing all instances of k^μ with $\frac{k^\mu}{T}$ in the above derivation. Keeping terms up to $N_2 = 3$, to improve convergence of the series for $\delta n_{\mathbf{k}}$, two functions were choses. In the low $x = \frac{k\cdot u}{T}$ limit, $\mathscr{G}_{\mathbf{k}} = \frac{1}{0.1+x}$, whereas $\mathscr{G}_{\mathbf{k}} = \frac{1}{(0.1+x)^4}$ is present in the high x region. Collecting powers of x after expanding out the series $\sum_{n=0}^{N_2} H^{(2)}_{n,\mathbf{k}} \frac{\eta_n}{\eta}$, one can derive Eq. (11). Furthermore, we have verified that the $\delta n_{\mathbf{k}}$ in Eq. (11) has converged by going to higher $N_2 = 4$ order, without significantly changing the coefficients the power series of x. Note that the coefficients in Eq. (11) were computed assuming that all chemical potentials are set to zero. If that is not the case, which happens when net baryon number diffusion is considered for example, then the coefficients depend on the chemical potential. Lastly note that setting $\mathscr{G}_{\mathbf{k}} = 1$, and letting $N_2 = 0$, recovers the original I-S viscous correction.

We conclude this Appendix with the following two remarks regarding $\delta n_{\mathbf{k}}$:

- Using perturbative QCD (pQCD) to derive $\delta n_{\mathbf{k}}$ would not be suitable. For one, the shear viscosity η_0 obtained through pQCD would be very large [8] (and possibly also leading to very large η_n). Implementing such a large η_0 in a hydrodynamical simulation would not only prevent any fit to experimental data, but would in fact violate the small Knudsen and inverse Reynolds numbers assumption of dissipative hydrodynamics.

- If one is to apply the above procedure to the hadronic sector, not only is the mass of hadrons participating in a particular interaction needed, but also the scattering cross section (or matrix element) associated with that particular interaction. So, every single hadron would have its own $\delta n_{\mathbf{k}}$. Given that a multitude of hadronic interaction cross sections are simply not know experimentally (and are poorly constrained theoretically), there is very little incentive to systematically expand $\delta n_{\mathbf{k}}$ in the hadronic sector. This is further reinforced with the fact that the viscous correction from the 14-moment approximation in the hadronic sector is already small in our calculations using $\eta/s = 1/(4\pi)$.

Appendix B: Effects of δR corrections on the differential dilepton yield of the QGP sector

In the light of the viscous correction to the quark distribution function in the QGP derived in the previous Appendix, it is instructive to investigate the manner in which the differential dilepton yield is modified. To that end, similar to the ratio A defined in Eq. (14), consider the quantity

$$\begin{aligned} \frac{\delta N}{N_0} &= \frac{\left|\langle \int_a^b p_T dp_T \int d\phi dy_s \tau d\eta_s \frac{d^4\delta R}{d^4 p}\rangle_{\rm ev}\right|}{\langle \int_a^b p_T dp_T \int d\phi dy_s \tau d\eta_s \frac{d^4 R_0}{d^4 p}\rangle_{\rm ev}} \\ &= \frac{\left|\frac{d\delta N}{dMdydxd\tau}(M, a, b, y = 0)\right|}{\frac{dN_0}{dMdydxd\tau}(M, a, b, y = 0)} \end{aligned} \tag{B1}$$

where y is the momentum rapidity whereas y_s is the space-time y-coordinate. Eq. (B1) quantifies the size of the contribution of the QGP yield coming from the anisotropic correction to the rate relative to the ideal rate [50].

The behavior of $\delta N/N_0$ depicted in Figs. 15 and 16 can be understood as an interplay between the decay of the envelope function b_2 in Eq. (13) and the growth of the term $\frac{p^\alpha p^\beta \pi_{\alpha\beta}}{2T^2(\epsilon+P)}$, which is best decribed through the ratio A

[4] Note that this approximation is not valid in the hadronic sector, where all colliding particles are massive.

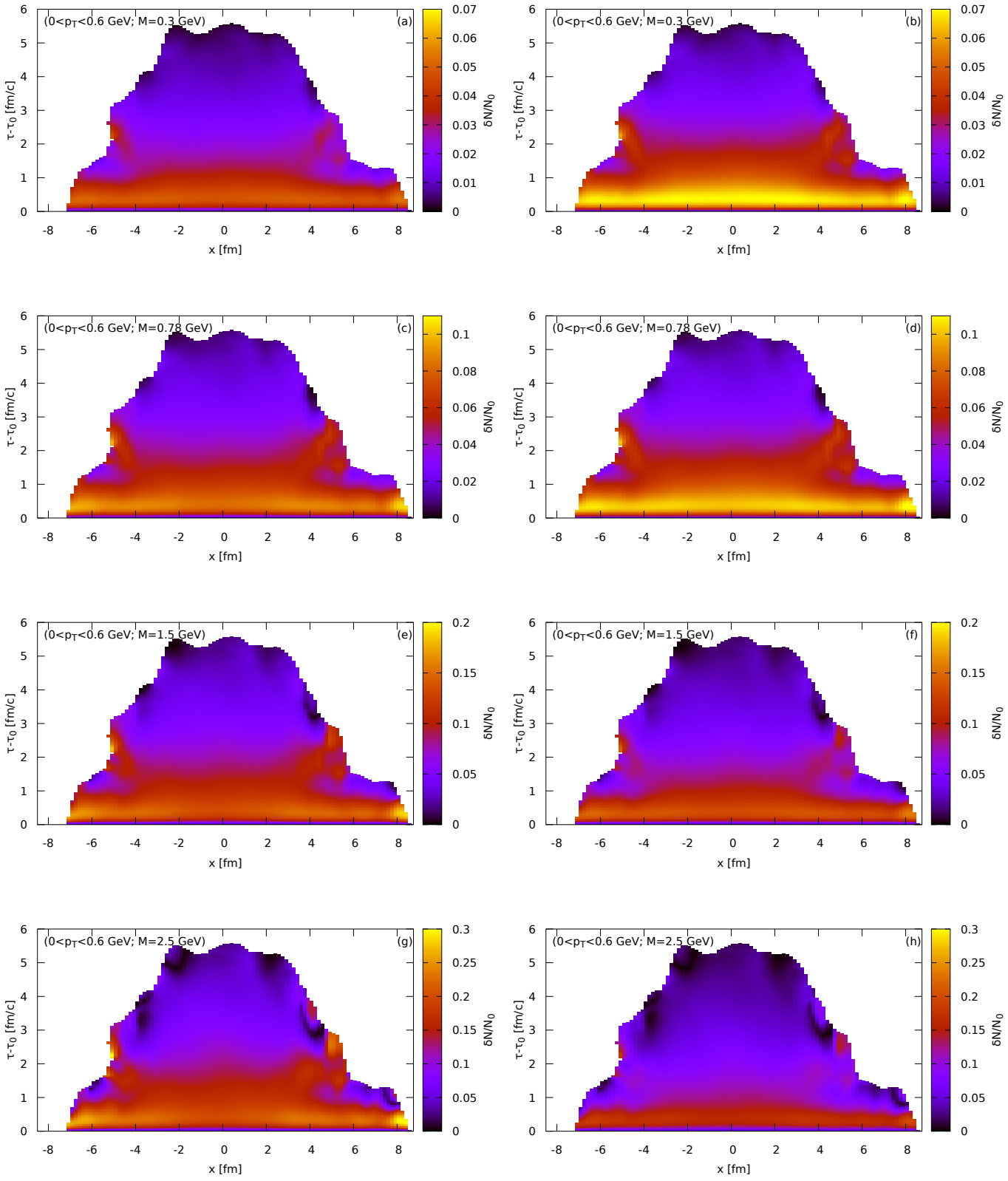
(0<pT<0.6 GeV; M=0.3 GeV) (a)
(0<pT<0.6 GeV; M=0.3 GeV) (b)
(0<pT<0.6 GeV; M=0.78 GeV) (c)
(0<pT<0.6 GeV; M=0.78 GeV) (d)
(0<pT<0.6 GeV; M=1.5 GeV) (e)
(0<pT<0.6 GeV; M=1.5 GeV) (f)
(0<pT<0.6 GeV; M=2.5 GeV) (g)
(0<pT<0.6 GeV; M=2.5 GeV) (h)
τ-τ0 [fm/c]
x [fm]
δN/N0

FIG. 15: (Color online) The size of the viscous contribution to the dilepton yield in the QGP relative to its ideal (inviscid) dilepton production. Left column: $\delta N/N_0$ using the I-S δR. Right column: $\delta N/N_0$ using the constant cross section δR.

in Eq. (14). For a fixed M, the A changes slowly with p_T while the term $\frac{p^\alpha p^\beta \pi_{\alpha\beta}}{2T^2(\epsilon+P)}$ grows quadratically with p_T,[5] whereas for a fixed p_T since the envelope decays $1/(p\cdot u)$ the quadratic growth from the term $\frac{p^\alpha p^\beta \pi_{\alpha\beta}}{2T^2(\epsilon+P)}$ is suppressed. The overall result is that $\delta N/N_0$ grows faster in the p_T-direction than M-direction, as can be seen in Figs. 15 and 16 and is consistent with the fact that A has a stronger energy dependence than three-momentum dependence.

The behavior of $\delta N/N_0$ as a function of p_T at low invariant mass and low p_T, resembles that of photons previously investigated in [50]. Like in the photon case, the size of the viscous correction is less than 14% throughout the entire evolution for $p_T < 1.6$ GeV. Viscous corrections only become large at early times with relatively high momenta $1.6 < p_T < 2.8$ GeV. This is especially true near the edges of the QGP sector in the x-direction, as is the case for photons as well [50]. Furthermore, the largest contributions from $\delta N/N_0$ for the low invariant mass region are happening at high p_T and at early times. Therefore these contributions will not significantly affect the p_T integrated $v_2(M)$ at low invariant masses, whose biggest contribution is coming from the low p_T [45] and late times sector (recall Fig. 6). The constant cross section δR in the QGP sector will however play a more important role as far as the p_T-integrated $v_2(M)$ at higher invariant masses are concerned (and can be seen in the right column of Fig. 16), where an improved description for the δR generates a more reliable $v_2(M)$ result.

Having discussed the effects of constant cross section δR in the temperature independent η/s, it is instructive to look at how $\delta N/N_0$ behaves once η/s is temperature dependent. In particular, we consider linear $\eta/s(T)$ with the highest slope in Fig. 17. For a low invariant mass $M = 0.3$ GeV and $p_T < 1.6$ GeV, the maximum δN correction to the differential dilepton yield is $\sim 18\%$ whereas at a higher invariant mass $M = 1.5$ GeV, the maximum δN correction raises to $\sim 29\%$. These percentages are sizable but not alarming. At higher momenta $1.6 < p_T < 2.8$ GeV, the δN correction does significantly increase, however $\delta N/N_0 < 1$ still holds, which is encouraging.

It should be emphasized one last time that the effects on the total $v_2(M)$ that were explored Section IV, are originating from the HM sector of the medium where viscous corrections to the dilepton rate are small and therefore effects seen on the total $v_2(M)$ are mostly independent of said corrections. The QGP only plays an important role once $M \geq 1.5$ GeV, and the discussion within this Appendix highlights the manner in which QGP dilepton production is modified owing to the constant cross section δR relative to the I-S one.

[1] U. Heinz and R. Snellings, Ann. Rev. Nucl. Part. Sci. **63**, 123 (2013), arXiv:nucl-th/1301.2826.
[2] C. Gale, S. Jeon, and B. Schenke, Int. J. Mod. Phys. **A28**, 1340011 (2013), [arXiv:nucl-th/1301.5893].
[3] P. Romatschke and U. Romatschke, Phys. Rev. Lett. **99**, 172301 (2007), 0706.1522.
[4] C. Shen, S. A. Bass, T. Hirano, P. Huovinen, Z. Qiu, H. Song, and U. Heinz, J. Phys. **G38**, 124045 (2011), 1106.6350.
[5] S. Ryu, J. F. Paquet, C. Shen, G. S. Denicol, B. Schenke, S. Jeon, and C. Gale, Phys. Rev. Lett. **115**, 132301 (2015), 1502.01675.
[6] C. Gale, Landolt-Bornstein **23**, 445 (2010), 0904.2184.
[7] L. P. Csernai, J. Kapusta, and L. D. McLerran, Phys. Rev. Lett. **97**, 152303 (2006), nucl-th/0604032.
[8] P. B. Arnold, G. D. Moore, and L. G. Yaffe, JHEP **05**, 051 (2003), [arXiv:hep-ph/0302165].
[9] M. Prakash, M. Prakash, R. Venugopalan, and G. Welke, Phys. Rept. **227**, 321 (1993).
[10] M. I. Gorenstein, M. Hauer, and O. N. Moroz, Phys. Rev. **C77**, 024911 (2008), [arXiv:nucl-th0708.0137].
[11] K. Itakura, O. Morimatsu, and H. Otomo, Phys. Rev. **D77**, 014014 (2008), [arXiv:hep-ph/0711.1034].
[12] J. Noronha-Hostler, J. Noronha, and C. Greiner, Phys. Rev. Lett. **103**, 172302 (2009), [arXiv:nucl-th/0811.1571].
[13] C. Greiner, J. Noronha-Hostler, and J. Noronha, PoS **BORMIO2011**, 033 (2011), arXiv:nucl-th/1105.1756.
[14] N. Christiansen, M. Haas, J. M. Pawlowski, and N. Strodthoff, Phys. Rev. Lett. **115**, 112002 (2015), 1411.7986.
[15] H. Niemi, K. J. Eskola, and R. Paatelainen, Phys. Rev. **C93**, 024907 (2016), [arXiv:hep-ph/1505.02677].
[16] G. Denicol, A. Monnai, and B. Schenke (2015), [arXiv:nucl-th/1512.01538].
[17] G. Denicol, A. Monnai, S. Ryu, and B. Schenke, in *25th International Conference on Ultra-Relativistic Nucleus-Nucleus Collisions (Quark Matter 2015) Kobe, Japan, September 27-October 3, 2015* (2015), [arXiv:nucl-th/1512.08231], URL `http://inspirehep.net/record/1411485/files/arXiv:1512.08231.pdf`.
[18] H. Niemi, G. S. Denicol, P. Huovinen, E. Molnar, and D. H. Rischke, Phys. Rev. Lett. **106**, 212302 (2011).
[19] P. Huovinen and P. Petreczky, Nucl. Phys. **A837**, 26 (2010), [arXiv:hep-ph/0912.2541].
[20] H. Bebie, P. Gerber, J. Goity, and H. Leutwyler, Nucl. Phys. **B378**, 95 (1992).
[21] T. Hirano and K. Tsuda, Phys. Rev. **C66**, 054905 (2002), [arXiv:nucl-th/0205043].
[22] W. Israel, Annals of Physics **100**, 310 (1976), ISSN 0003-4916, URL `http://www.sciencedirect.com/science/article/pii/0003491676900646`.

[5] Note that at the highest p_T, there is a slight suppression in the case of constant cross section δR relative to I-S δR owing to the envelope b_2 in Eq. (13).

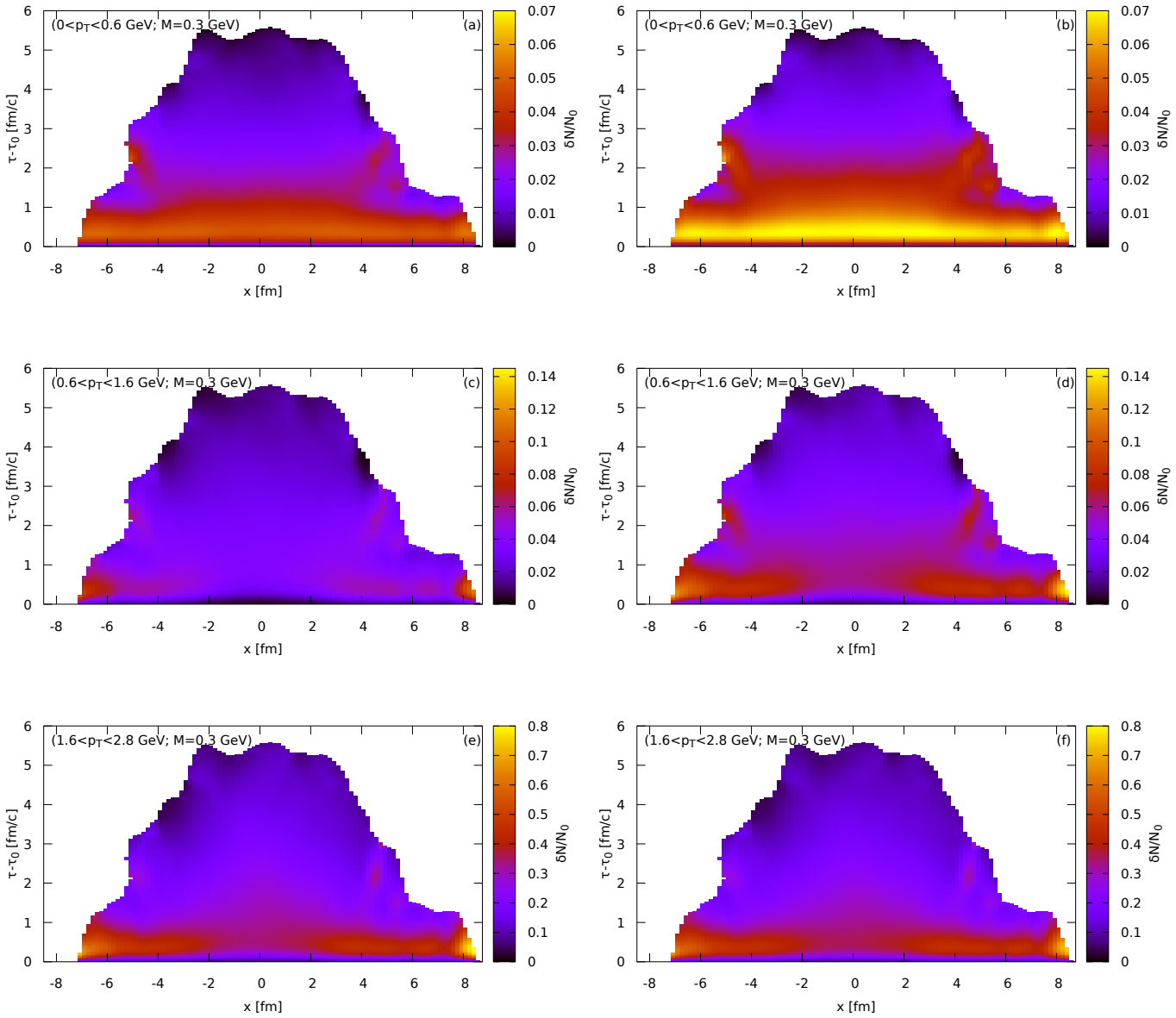

FIG. 16: (Color online) The size of the viscous contribution to the dilepton yield in the QGP relative to its ideal (inviscid) dilepton production for a medium with constant $\eta/s = 1/(4\pi)$. Left column: $\delta N/N_0$ using the I-S δR. Right column: $\delta N/N_0$ using the constant cross section δR.

[23] W. Israel and J. Stewart, Annals Phys. **118**, 341 (1979).
[24] R. Baier, P. Romatschke, D. T. Son, A. O. Starinets, and M. A. Stephanov, JHEP **04**, 100 (2008), 0712.2451.
[25] G. S. Denicol, H. Niemi, E. Molnar, and D. H. Rischke, Phys. Rev. **D85**, 114047 (2012), [Erratum: Phys. Rev.D91,no.3,039902(2015)], [arXiv:nucl-th/1202.4551].
[26] G. Denicol, J. Phys. **G41**, 124004 (2014).
[27] A. Nakamura and S. Sakai, Phys. Rev. Lett. **94**, 072305 (2005), [arXiv:hep-lat/0406009].
[28] H. B. Meyer, Nucl. Phys. **A830**, 641C (2009), 0907.4095.
[29] M. Haas, L. Fister, and J. M. Pawlowski, Phys. Rev. **D90**, 091501 (2014), 1308.4960.
[30] H. Marrochio, J. Noronha, G. S. Denicol, M. Luzum, S. Jeon, et al. (2013), [arXiv:nucl-th/1307.6130].
[31] J. Bjorken, Phys. Rev. **D27**, 140 (1983).
[32] G. Vujanovic, J.-F. Paquet, G. S. Denicol, M. Luzum, S. Jeon, and C. Gale, Phys. Rev. **C94**, 014904 (2016), [arXiv:nucl-th/1602.01455].
[33] F. Cooper and G. Frye, Phys. Rev. **D10**, 186 (1974).

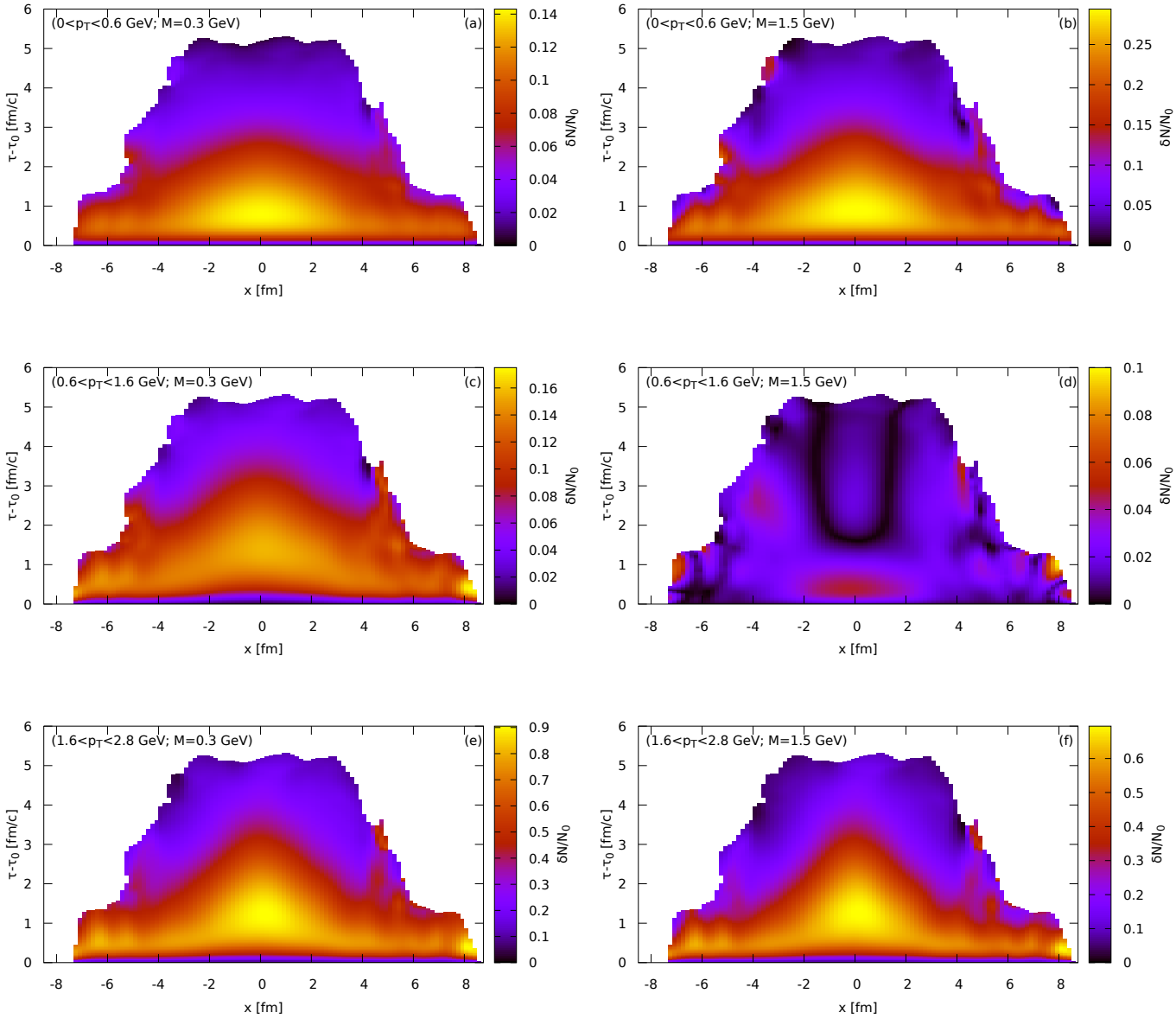

FIG. 17: (Color online) The size of the viscous contribution to the dilepton yield in the QGP relative to its ideal (inviscid) dilepton production using the constant cross section δR for a medium with linear $\eta/s(T)$ and slope $m = 0.5516$. The left column plots $\delta N/N_0$ for $M = 0.3$ GeV whereas the right column plots the same quantity at $M = 1.5$ GeV.

[34] D. Teaney, Phys. Rev. **C68**, 034913 (2003), [arXiv:nucl-th/0301099].
[35] J. Sollfrank, P. Koch, and U. W. Heinz, Z. Phys. **C52**, 593 (1991).
[36] M. Laine, JHEP **1311**, 120 (2013), [arXiv:hep-ph/1310.0164].
[37] I. Ghisoiu and M. Laine, JHEP **1410**, 83 (2014), [arXiv:hep-ph/1407.7955].
[38] J. Ghiglieri and G. D. Moore, JHEP **1412**, 029 (2014), [arXiv:hep-ph/1410.4203].
[39] S. Caron-Huot, P. Kovtun, G. D. Moore, A. Starinets, and L. G. Yaffe, JHEP **0612**, 015 (2006), [arXiv:hep-th/0607237].
[40] H.-T. Ding, A. Francis, O. Kaczmarek, F. Karsch, E. Laermann, et al., Phys. Rev. **D83**, 034504 (2011), [arXiv:hep-lat/1012.4963].
[41] O. Kaczmarek, E. Laermann, M. Mller, F. Karsch, H. T. Ding, S. Mukherjee, A. Francis, and W. Soeldner, PoS **ConfinementX**, 185 (2012), [arXiv:hep-lat/1301.7436].
[42] G. Gounaris and J. Sakurai, Phys. Rev. Lett. **21**, 244 (1968).
[43] C. D. Roberts and A. G. Williams, Prog. Part. Nucl. Phys. **33**, 477 (1994), [arXiv:hep-ph/9403224].
[44] V. Eletsky, M. Belkacem, P. Ellis, and J. I. Kapusta, Phys. Rev. **C64**, 035202 (2001), [arXiv:nucl-th/0104029].

[45] G. Vujanovic, C. Young, B. Schenke, R. Rapp, S. Jeon, et al., Phys. Rev. **C89**, 034904 (2014), [arXiv:nucl-th/1312.0676].
[46] K. Dusling and S. Lin, Nucl. Phys. **A809**, 246 (2008), [arXiv:nucl-th/0803.1262].
[47] F. Geurts, Private Communication (2016).
[48] P. Jacobs and G. Roland, Private Communication (2016).
[49] S. R. de Groot, W. A. van Leeuwen, and C. G. van Weert, *Relativistic Kinetic Theory: Principles and Applications* (North-Holland; Elsevier, Amsterdam; New York, 1980).
[50] C. Shen, J.-F. Paquet, G. S. Denicol, S. Jeon, and C. Gale (2016), 1609.02590.